J. Electroanal. Chem., 170 (1984) 227–242
Elsevier Sequoia S.A., Lausanne – Printed in The Netherlands

THE OXYGEN EVOLUTION REACTION ON COBALT

PART I. REACTION ORDER EXPERIMENTS AND IMPEDANCE MEASUREMENTS

H. WILLEMS, A.G.C. KOBUSSEN *, J.H.W. DE WIT and G.H.J. BROERS

State University of Utrecht, Inorganic Chemistry Department, Croesestr. 77 A, 3522 AD Utrecht (The Netherlands)

(Received 8th August 1983; in revised form 19th January 1984)

ABSTRACT

It was found that the oxygen evolution reaction on cobalt in concentrated KOH solutions can be described differently for low and high overpotentials. In the overpotential range from 150 to 280 mV, the reaction has a Tafel slope of approximately 40 mV and a reaction order with respect to the KOH activity at constant overpotential of 0.6; in the overpotential range from 300 to 400 mV, the reaction has a slope of 60–80 mV and a reaction order of 0.3–0.4. The effective capacitance showed a slight maximum at the potential where it is proposed that the character of the rate-determining step changes. By incorporating the water activity (which changes for changing hydroxyl ion activities) in the calculations, an extra diagnostic criterion was obtained. From our results we propose a modified Krasil'shchikov reaction mechanism for the low overpotential region.

INTRODUCTION

As early as 1922 the metal cobalt was investigated as an electrode material for oxygen evolution by Grube and Feucht [1]. Later, a large group of cobalt-containing oxides, such as $La_{0.5}Ba_{0.5}CoO_3$ [2], $NiCo_2O_4$ [3] and Co_3O_4 [4], also became of interest because they combine a high catalytic activity of Co with a reasonable stability of the electrode towards oxygen evolution. However, the oxygen evolution reaction on cobalt itself has never been studied in detail. Mostly the Krasil'shchikov [5] mechanism is used to describe the oxygen evolution reaction on nickel(-oxide) and cobalt(-oxide) electrodes:

$$OH^- \leftrightarrows OH_{ad} + e^- \quad (1)$$

$$OH^- + OH_{ad} \leftrightarrows O_{ad}^- + H_2O \quad (2)$$

* Present address: VEG-Gasinstituut n.v., Materials Research Department, P.O. Box 137, 7300 AC Apeldoorn, The Netherlands.

0022-0728/84/$03.00

$$O_{ad}^{-} \leftrightarrows O_{ad} + e^{-} \quad (3)$$

$$2\ O_{ad} \rightarrow O_2 \quad (4)$$

Depending on the rate-determining step chosen, this path can lead to a variety of Tafel slopes. Several authors have modified this reaction path to explain their experimental results. In our study of the oxygen evolution reaction on cobalt, we performed experiments to determine the reaction order of the hydroxyl ion at constant overpotential and, in addition, we measured the impedance response of this reaction in 6 *M* KOH.

The results of these experiments will be used to discuss the applicability of the Krasil'shchikov mechanism and its modifications to describe the oxygen evolution reaction on cobalt.

EXPERIMENTAL

A sample of spec pure cobalt metal (Merck) was ground to obtain a flat surface and then embedded in two-component Technovit resin to obtain a circular rotating disk electrode. Before use, the electrode was polished with an 8 μm diamond paste. All experiments were carried out in a three-compartment cell [6] and were performed at room temperature. The cell was continuously flushed with N_2 gas. The electrode was rotated at a speed of approximately 200 rad/s.

Potentials were measured against a Hg/HgO reference electrode in the same solution and are given with respect to the ROE (reversible oxygen electrode) in the same solution. Since the dependence of the equilibrium potential on the activities of hydroxyl ion and water is the same for the ROE and this reference electrode, the measured potential difference is independent of the water and hydroxyl activities (which means that the reaction order is measured at constant overpotential). From thermodynamic data on the oxidation of Hg one obtains:

$$E(O_2, 1\ \text{atm}) = 303 - 0.56(T - 298) \quad \text{mV} \quad (1)$$

where T is the temperature in kelvin.

Electrolyte solutions were prepared from analytical grade 85% KOH pellets and doubly-distilled water. The hydroxyl ion concentration was determined by titration.

Anodic polarization curves were obtained potentiostatically with a stepping potentiometer (with a step size of 10 mV at a rate of 4 steps/h). Ohmic resistances were corrected with an improved version of the automatic current interruptor/compensator published by Moors and Demedts [7]. All current densities are based on the geometrical surface area (0.273 cm^2).

The cyclic voltammetric measurements (triangular sweeps) were performed in the same cell using a voltage scan generator with scan rates of 100, 33 and 10 mV/s.

All impedance measurements were carried out in 6 *M* KOH at room temperature. Impedances were measured with a Solartron 1172 Frequency Response Analyzer (FRA) and the measurements were performed using the method described by Kobussen [8]; the circuit diagram is given in Fig. 1 for clarity. After corrections for

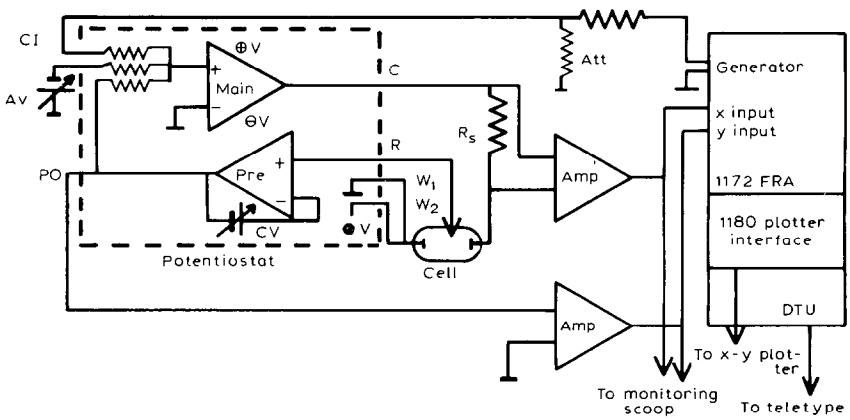

Fig. 1. System used for electrochemical impedance measurements.

the effective inductance of the cell (generally of the order of 100 nH), the data were fitted by a computer program to an electrical equivalent circuit by minimizing the sum of the absolute values of the complex squared differences between the measured and calculated impedances.

RESULTS

After the cobalt electrode was stabilized at a high overpotential ($\eta > 400$ mV), Tafel curves were measured in three different alkaline solutions (with molarities of 2.78 *M*, 4.84 *M* and 6.30 *M* KOH, and activities of 2.89, 8.87 and 18.40 mol/l, respectively). A typical Tafel plot in 4.84 *M* KOH is shown in Fig. 2. Notice the severe hysteresis at high overpotentials. On scanning from low to high overpotentials it was found that after a potential step the current tended to increase with time in the low overpotential range, while at high overpotentials the current tended to decrease with time. Scanning from high to low overpotentials resulted in the opposite behaviour. In all experiments two Tafel regions were discernible. From approximately 200 to 280 mV the slope appeared to be approximately 40 mV, while from approximately 300 to 400 mV the slope varied from 60 to 80 mV. In Fig. 3 the Tafel plots for three different alkaline solutions are shown (scanned from low to high overpotentials). For the lowest concentration (curve 3), it is seen that at high overpotentials ($\eta > 380$ mV) the Tafel behaviour no longer holds. In Fig. 4 a plot is shown of log i vs. the logarithm of the activity at four different overpotentials. The activities of the KOH solutions were calculated from the measured molarities and the appropriate activity coefficients as given by Akerlof and Bender [9]. The values of the slopes are given in Table 1 together with the Tafel slopes found. The reaction order was not different for decreasing or increasing potential.

Cyclic voltammetry was performed on a freshly polished cobalt electrode in 6 *M* KOH at sweep rates of 10, 33 and 100 mV/s. In Fig. 5, three peaks can be

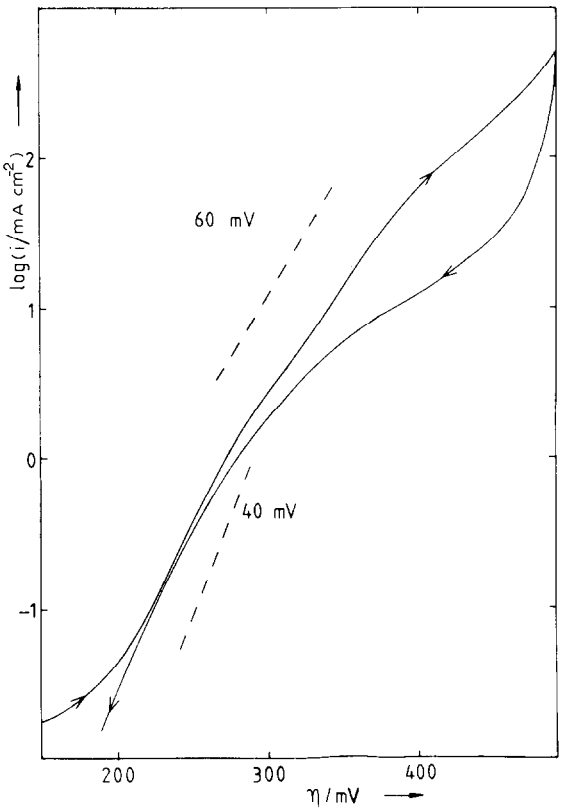

Fig. 2. Plot of the logarithm of the current density vs. the overpotential (iR-corrected) in the oxygen evolution range in 4.84 M KOH.

distinguished at −189, 35 and 240 mV overpotential, respectively (sweep rate 33 mV/s). The oxygen evolution range was scanned separately at 100 mV/s, as shown in Fig. 6. These results are in agreement with those of Burke et al. [10] and Gomez Meier et al. [11] who discussed this curve in detail.

The impedance measurements were performed on an "aged" cobalt electrode (charge passed approximately 10^5 C). The electrode was kept at the chosen potential for ca. 30 min and then the impedances were measured with frequencies from 10 kHz to 0.1 Hz. Then the potential was stepped to a new value (50 mV per step with increasing potential and 30 mV per step for decreasing potential) and was kept constant again. An example of an impedance measurement is given in Fig. 7 and it can be seen that the impedances lie on a semi-circle. The impedance data were fitted to the electrical equivalent circuit given in Fig. 8 by a least-squares method, as was discussed in detail by Kobussen [8]. A cpa (constant phase angle) was used because the impedances were not on a semi-circle whose centre lay on the Z'-axis. The

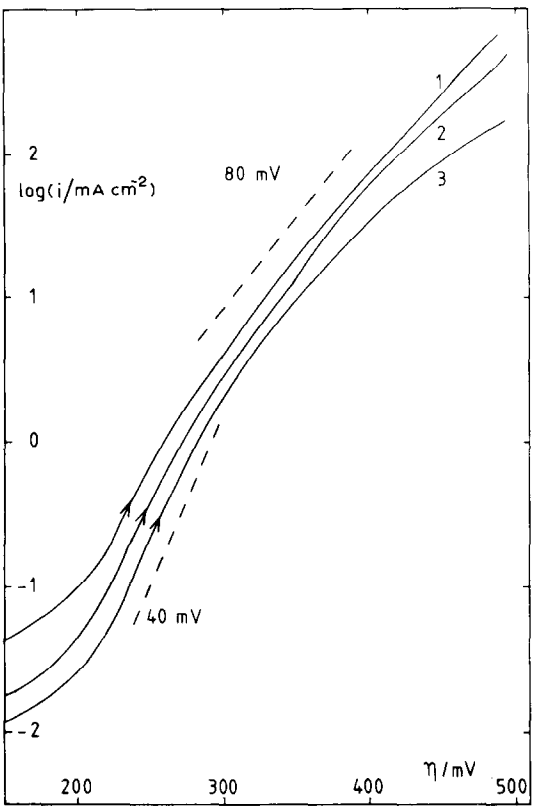

Fig. 3. Current density responses for three different hydroxyl concentrations going from low to high overpotentials (*iR*-corrected). (1) 6.30 *M*; (2) 4.84 *M*; (3) 2.78 *M*.

admittance of a cpa can be formulated as:

$$Y_{\text{cpa}} = (j\omega C)^{p} = A(j\omega)^{p} \tag{2}$$

TABLE 1

Tafel slopes measured for oxygen evolution on cobalt and reaction orders towards OH^- at constant overpotential

η/mV	$(d\eta/d \log i)$/mV	$(d \log i/d \log a)_\eta$
230	40–50	0.67
250	40–50	0.58
330	60–80	0.37
350	60–80	0.38

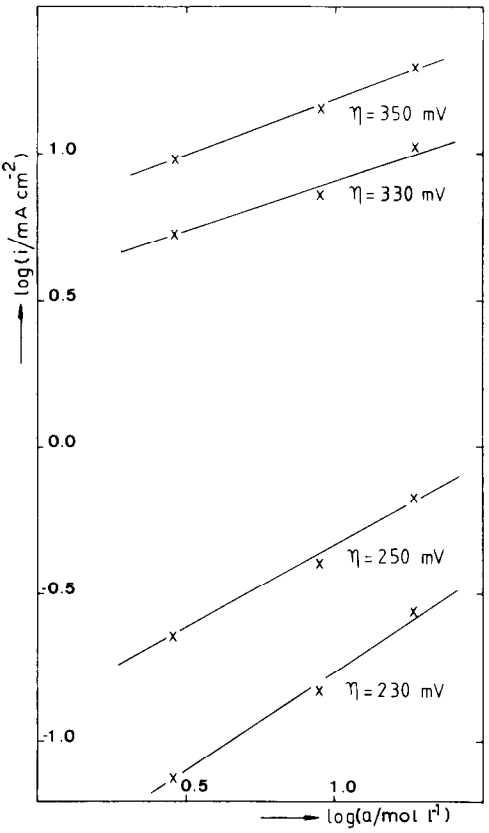

Fig. 4. Dependence of the current density on the hydroxyl ion activity at four different overpotentials, as indicated in the figure.

in which ω is the angular frequency and A and p are parameters to be determined experimentally. Effective capacitances can be calculated from the cpa parameters according to:

$$C_{\text{eff}} = (a)^{1/p} \tag{3}$$

A plot of C_{eff} vs. η is shown in Fig. 9. A slight maximum of C_{eff} is found between 250 and 280 mV. The highest and lowest capacitances differ by a factor of 3.

Another parameter obtained is the faradaic resistance R_{f}. This parameter can be used together with the dc current density to calculate the differential Tafel slope according to (when there is simple Tafel behaviour $i = i_0 \exp(2.303\ \eta/b)$):

$$b_{\text{diff}} \equiv \mathrm{d}\eta/\mathrm{d}\log i = 2.303 i_{\text{dc}} (\mathrm{d}\eta/\mathrm{d}i) = 2.303 i_{\text{dc}} R_{\text{f}} \tag{4}$$

A plot of b_{diff} vs. η is shown in Fig. 10. In this plot it is seen that b_{diff} is not really

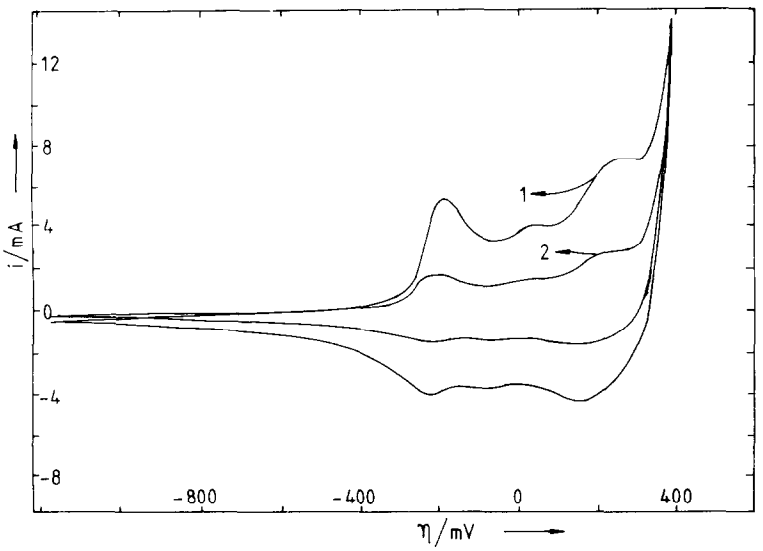

Fig. 5. Current response on a voltage scan with two different scan rates. (1) 33 mV/s; (2) 10 mV/s (not iR-corrected).

a constant although it remains between 40 and 50 mV in the overpotential range from 225 to 325 mV. But at low and high overpotentials, b_{diff} shows deviations from the expected behaviour. An alternative way of using R_f is given in Fig. 11 where the logarithm of $Y_f(=1/R_f)$ is plotted against η. Again if we assume simple Tafel

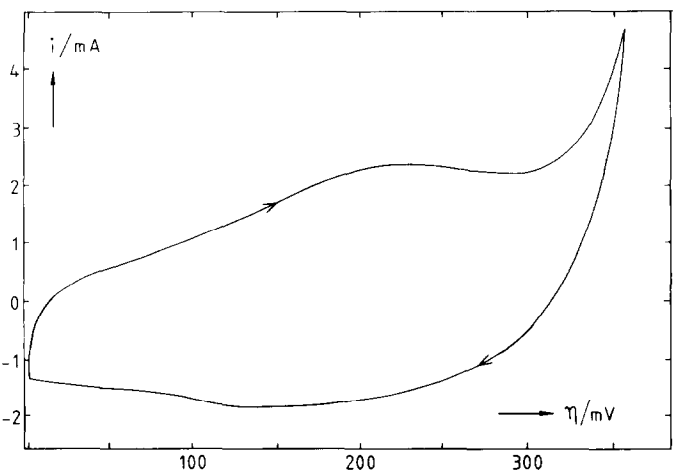

Fig. 6. Current response on a voltage scan in the area of oxygen evolution (scan rate 100 mV/s and not iR-corrected).

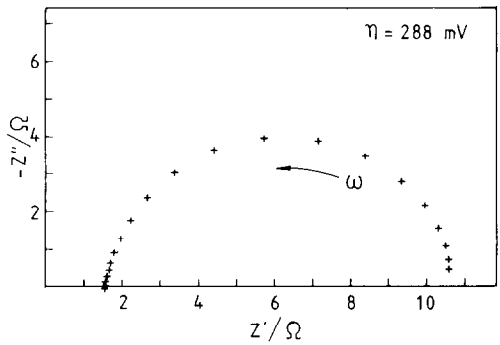

Fig. 7. Example of measured impedance data for $\eta = 288$ mV.

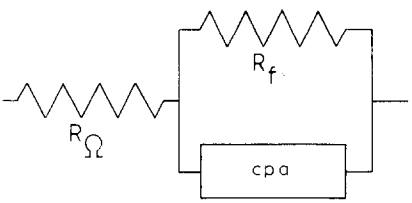

Fig. 8. Proposed electrical circuit diagram for fitting the measured impedance data.

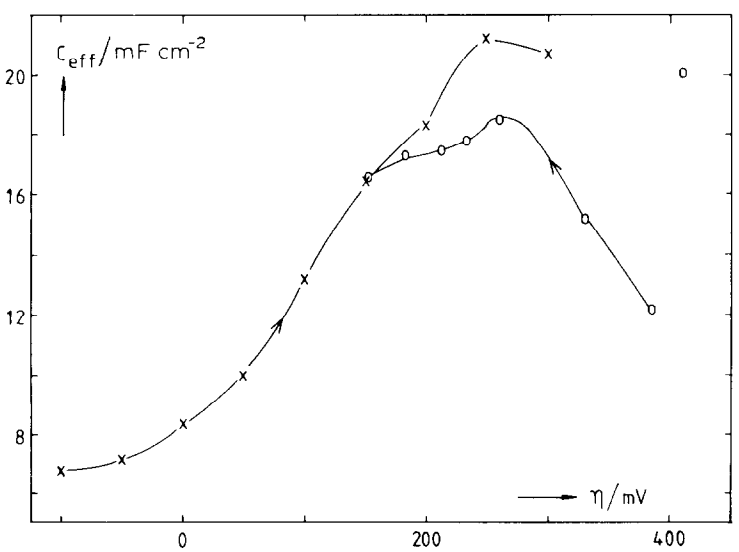

Fig. 9. Effective capacitances vs. the overpotential. (×) For increasing overpotential; (○) for decreasing overpotential.

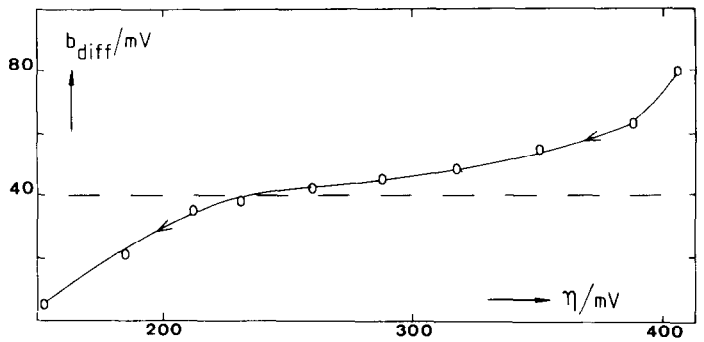

Fig. 10. Differential Tafel slopes calculated from the faradaic resistance vs. the overpotential (dashed line is 40 mV).

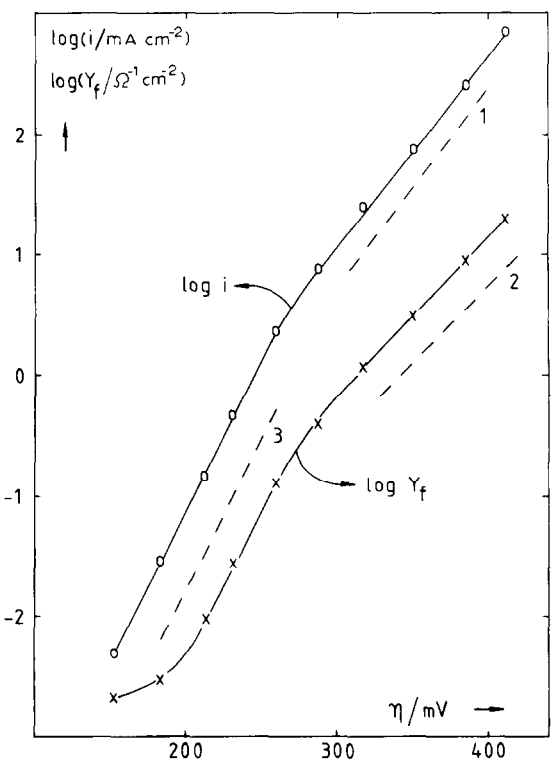

Fig. 11. Results of the fit procedure on the impedance data. (×) Logarithm of the faradaic resistance for decreasing overpotential; (○) logarithm of the current density for decreasing overpotential. Dashed lines indicate: (1) 80 mV; (2) 60 mV; (3) 40 mV.

TABLE 2

"Apparent" exchange current densities i_0: (1) calculated from the current densities; (2) calculated from the faraday resistance Y_f.

	i_0/mA cm^{-2}	
	1	2
High overpotentials	2.0×10^{-4}	3.6×10^{-3}
Low overpotentials	7.5×10^{-7}	7.3×10^{-7}

TABLE 3

Results of the fit procedure on the impedance data for increasing overpotential

η/mV	i/mA cm^{-2}	C_{eff}/mF cm^{-2}	Y_f/Ω^{-1} cm^{-2}	R_Ω/Ω	b_{diff}/mV	φ/°
−100	~ 0	7.1	1.08×10^{-3}	1.503	–	13.3
−50	~ 0	7.4	0.78×10^{-3}	1.493	–	12.6
0	~ 0	8.7	0.52×10^{-3}	1.491	–	12.8
50	~ 0	10.4	0.19×10^{-3}	1.509	–	12.9
100	0.081	13.7	0.01×10^{-3}	1.500	1348	13.0
150	0.095	18.1	0.66×10^{-3}	1.493	331	13.1
200	0.238	18.9	2.18×10^{-3}	1.492	252	13.1
247	1.062	22.0	8.08×10^{-2}	1.493	30	10.6
300	24.52	20.4	1.16	1.494	49	10.0

TABLE 4

Results of the fit procedure on the impedance data for decreasing overpotential

η/mV	i/mA cm^{-2}	C_{eff}/mF cm^{-2}	Y_f/Ω^{-1} cm^{-2}	R_Ω/Ω	b_{diff}/mV	φ/°
411	709.0	21.0	20.1	1.543	81.2	28.1
385	258.0	12.6	9.24	1.531	64.4	12.1
350	77.1	13.7	3.20	1.527	55.6	9.9
317	25.3	15.8	1.18	1.523	49.4	9.0
288	7.84	18.1	0.397	1.525	45.5	8.0
260	2.41	19.1	0.130	1.520	42.8	8.5
231	0.462	18.5	0.0278	1.496	38.3	10.3
213	0.147	18.1	0.00963	1.496	35.2	11.0
183	0.029	17.9	0.00290	1.487	23.3	11.3
153	0.005	17.3	0.00209	1.482	5.5	11.1

behaviour, the slope of this plot must also give the Tafel slope:

$$Y_f = \mathrm{d}i/\mathrm{d}E = \{2.303 i_0 \exp(2.303\eta/b)\}/b \tag{5}$$

which gives:

$$\log Y_f = \eta/b + \log(2.303 i_0/b) \tag{6}$$

In the same figure the dc current densities are given and one can see that the slopes of the two lines are not the same for high overpotentials. This implies that either the current does not follow a simple Tafel law or that the so-called Y_f is in reality much more complicated. It is also seen that for low overpotentials log Y_f tends to go to a constant value. From eqn. (6) it is clear that from a plot of log Y_f vs. η a faradaic current density may also be determined. From Fig. 11 two overpotential regions may be distinguished, each with different exchange current densities. In Table 2 all the exchange current densities are given. Note that the exchange current densities from the current measurements (1) and from impedance data (2) are approximately equal for low overpotentials and are different for high overpotentials.

All the impedance results are summarized in Tables 3 and 4, and these show that the inclination of the cpa admittance ($\varphi°$) remains fairly constant (10–12°).

DISCUSSION

All our experimental results indicate that the oxygen evolution reaction (OER) on Co may be separated into two parts: one in the overpotential range from 150 to 280 mV, and one from 300 to 400 mV. Both potential regions will be discussed separately.

Low overpotential

The Tafel slope found from steady-state measurements as well as from impedance measurements is ca. 40 mV and is the same as that found for nickel at low overpotentials (see, for example, ref. 12).

The current density i is proportional to the square root of the hydroxyl ion activity a at constant overpotential (Fig. 4 and Table 1). From these measurements it follows that for low overpotentials the anodic current density may be described by:

$$i = k_1 (a_{OH^-})^{0.5} \exp(1.5\eta F/RT) \tag{7}$$

Many authors have proposed mechanisms for the OER on Co and Co-containing oxides. They have all used the Krasil'shchikov mechanism [5] as a basis with one or two modifications. Burke et al. [10] have proposed the following mechanism for the OER on Co:

$$OH^- \leftrightarrows OH_{ad} + e^- \tag{I.1}$$

$$OH_{ad} + OH^- \leftrightarrows O_{ad}^- + H_2O \tag{I.2}$$

$$CoO_2 + O_{ad}^- \rightarrow CoO_2 \cdot O + e^- \tag{I.3}$$

$$CoO_2 \cdot O \rightarrow CoO_2 + O_{ad} \tag{I.4}$$

$$2\ O_{ad} \rightarrow O_2 \tag{I.5}$$

When step (I.3) is taken as the rate-determining step (rds) and with steps (I.1) and (I.2) at quasi-equilibrium, low coverages of the intermediates with Langmuir-type

adsorption, and the steps following the rds fast, the current density can be described by:

$$i = K(a_{OH^-})^2 \exp[(3/2)E] \tag{8}$$

with K a constant independent of the potential and the hydroxyl ion activity, and E the dimensionless potential difference across the interface ($= \varepsilon F/RT$). The overpotential can be defined in terms of the equilibrium potential ε^e and ε, the potential of the electrode:

$$\eta = \varepsilon - \varepsilon^e = \varepsilon - \left\{\varepsilon^\circ - RT/4F \ln\left[(a_{OH^-})^4/(a_{H_2O})^2 pO_2\right]\right\} \tag{9}$$

Substituting eqn. (9) in eqn. (8) gives:

$$i = k(a_{OH^-})^{0.5} \exp[(3/2)\eta F/RT] \tag{10}$$

which gives a Tafel slope of 40 mV and a reaction order (dlog i/dlog a_{OH^-}) at constant overpotential of 0.5.

Rasiyah and Tseung [13] took into account the formation of higher oxides on the surface of $NiCo_2O_4$. They proposed the following OER mechanism:

$$MO + OH^- \leftrightarrows MOOH + e^- \tag{II.1}$$

$$MOOH + OH^- \rightarrow MO_2 + H_2O + e^- \tag{II.2}$$

$$2\,MO_2 \rightarrow 2\,MO + O_2 \tag{II.3}$$

M in this case would be Co. When the second step is rate-determining, this mechanism also gives a Tafel slope of 40 mV and a reaction order of 0.5 (with step II.1 at quasi-equilibrium and step II.3 fast while the intermediates show low coverage).

Rasiyah and Tseung also proposed a mechanism for the OER on Li-coped Co_3O_4 [14]:

$$T + OH^- \leftrightarrows TOH + e^- \tag{III.1}$$

$$TOH + OH^- \leftrightarrows TO^- + H_2O \tag{III.2}$$

$$TO^- + M \rightarrow T\text{–}O\text{–}M + e^- \tag{III.3}$$

$$2\,T\text{–}O\text{–}M \rightarrow 2\,T + 2\,M + O_2 \tag{III.4}$$

where T is trivalent cobalt and M is divalent or trivalent cobalt. This mechanism, however, resembles mechanism (I) if we neglect the way the intermediates are bonded/adsorbed and neglect the steps following (III.3). Our experimental results are compatible with this mechanism provided that the third step is rate-determining. So two possible mechanisms fit a Tafel slope of 40 mV and a reaction order of 0.5.

Until this point, we have assumed that the activity of water, a_{H_2O}, is constant and independent of the hydroxyl activity, a_{OH^-}. The activity of water may be calculated from the vapour pressures of different KOH solutions according to:

$$(a_{H_2O})_{ref}/(a_{H_2O})_m = p_{H_2O}(\text{ref})/p_{H_2O}(\text{m}) \tag{11}$$

where ref refers to pure water and m refers to the solution with a known hydroxyl activity. In Fig. 12 a plot is shown of the logarithm of the hydroxyl ion activity against the logarithm of the water activity. It is clear that the water activity is not constant. In the area of interest ($0.5 < \log(a_{OH^-}) < 1.5$), the slope of the plot is almost constant and gives:

$$\{\mathrm{d}\log(a_{H_2O})\}/\{\mathrm{d}\log(a_{OH^-})\} = -1/3 \tag{12}$$

Now the reaction orders towards hydroxyl ion and water may be combined into one effective reaction order for our experiments since:

$$\{\mathrm{d}\log i/\mathrm{d}\log a_{OH^-}\}_{\mathrm{eff},\eta} = n + m(\mathrm{d}\log a_{H_2O}/\mathrm{d}\log a_{OH^-}) \tag{13}$$

where n and m are the reaction orders for hydroxyl ion and water, respectively. If we take this into account in calculating the reaction order, we obtain for mechanisms (I) and (III):

$$i = k(a_{OH^-})^{0.5}(a_{H_2O})^{-1/4}\exp[(3/2)\eta F/RT] \tag{14}$$

By applying eqn. (13), the effective reaction order towards the hydroxyl activity at constant overpotential is calculated to be:

$$\{\mathrm{d}\log(i)/\mathrm{d}\log(a_{OH^-})\}_{\mathrm{eff},\eta} = 0.58$$

This would explain the experimental results even better because the mean slope found in our experiments was 0.62 for low overpotentials.

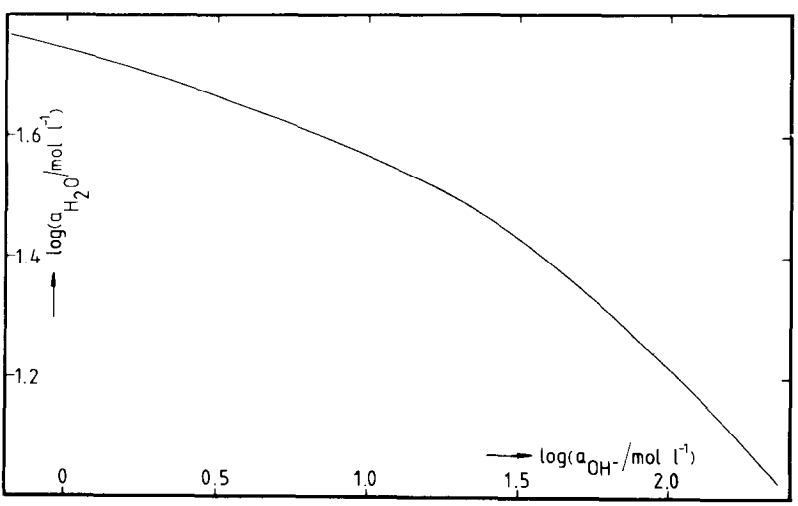

Fig. 12. Logarithm of the activity of water as a function of the logarithm of the activity of the hydroxyl ion ($T = 20\,^\circ\mathrm{C}$).

In the same way, mechanism (II) can be evaluated, which gives:

$$i = k'(a_{OH^-})^{0.5}(a_{H_2O})^{3/4} \exp[(3/2)\eta F/RT] \quad (15)$$

and so

$$\{\mathrm{d}\log(i)/\mathrm{d}\log(a_{OH^-})\}_{\mathrm{eff},\eta} = 0.25$$

This result is not in accordance with our experiments.

A first conclusion drawn is that when the water activity is taken into account, mechanism (II) obviously does not hold and the experimental results are reasonably explained by mechanism (I) or (III). As to the nature of the adsorption sites, the following may be concluded. From Figs. 5 and 6 it is seen that in the low overpotential range an oxidation of the surface takes place. This oxidation step is generally attributed to the formation of CoO_2 [10,11,15]. Let us assume that this formation of a higher oxide at the surface is responsible for the change in the OER on cobalt at 280 – 300 mV overpotential. Now we suggest that the adsorption of the intermediates takes place at either a divalent cobalt site or a trivalent cobalt site. The activity of these sites should remain constant in this overpotential range and the oxidation of the surface to CoO_2 only plays a role above this range when the coverage of CoO_2 increases. So mechanism (III) can give a more appropriate explanation of our experimental results then mechanism (I).

High overpotentials

At higher overpotentials the situation is more complex. The Tafel slope is no longer constant but varies from 60 to 80 mV, which is in reasonable agreement with the Tafel slope found by Burke et al. [10] on Co, and the Tafel slopes for other Co-containing compounds such as Fe-supported Co_3O_4 [4] and Li-doped Co_3O_4 [14], $NiCo_2O_4$ [3] and $La_{0.5}Ba_{0.5}CoO_3$ [2] which are all 60 mV. Mechanism (I) or (III) with the second step as rate-determining will indeed give a Tafel slope of 60 mV but then the reaction order does not fit (and the coverage of OH_{ad} must be low at the same time, which is not very likely at these high overpotentials). Now at high overpotentials it becomes more difficult to decompose CoO_2. So if we assume that the fourth step is the rds and the coverage of OH_{ad} is almost at its maximum, then the current may be described by:

$$i = K(a_{H_2O})^{-0.5} \exp(\eta F/RT) \quad (16)$$

which gives an effective reaction order towards hydroxyl ion at constant overpotential of 0.17 and a Tafel slope of 60 mV. So mechanism (I) can explain the experimental results found in the classical way although not very satisfactorily. After all, this is not very surprising since, in connection with Fig. 11, it has already been concluded that the rate-determining process at high overpotentials is not Tafel-like in appearance. In their series of articles on the passivation of iron, Cahan and Chen [16–19] gave a totally different description of the OER. They stated that the oxygen

evolution on metal(-oxide) electrodes may be interpreted in terms of a potential-dependent conductivity of the metal-oxide surface layer rather than potential-dependent reaction kinetics. From Figs. 5 and 6 it is seen that there is an oxidation of the surface just before the change in the mechanism and this oxidation is generally attributed to the formation of CoO_2, which itself is a bad conductor and could thus give a poorly conducting surface layer. If this hypothesis is adopted, the variation of the Tafel slope could be explained by the dependence of the structure of the oxide layer (and consequently the conductivity) on the history of the electrode. Although stoichiometric CoO_2 is not known to exist as a stable bulk material, it may very well exist as an outer surface layer attached to suboxides of Co, especially under dynamic conditions. It is also known that CoO_2 is stabilized by intercalation of K^+ ions [20], which will also improve the conductivity.

Impedance results

The fit of the equivalent circuit of Fig. 8 is worse at high overpotentials. Still, within the accuracy of the measurements, no other equivalent circuit may be devised which gives a significant improvement of the fit.

The effective capacitance C_{eff} shows a maximum at ca. 280 mV, which is the overpotential region where the Tafel slope changes. Such a maximum was also found by Kobussen [8] on $La_{0.5}Ba_{0.5}CoO_3$ at a somewhat lower potential. We have shown in our previous publications [21,22] that an OER with a chemical rds following two electrochemical steps can lead to a maximum in the capacitance curve. But this maximum should be rather sharp which is not the case here. Oxidation of the surface layer also results in a maximum in the capacitance curve. In Figs. 5 and 6 it is seen that the oxidation peaks of the surface are very broad and a large background current exists. In Fig. 9 it is shown that the peak is very broad and that the capacitance below 150 mV overpotential is too high to be explained in terms of a double-layer capacitance. So we suggest here that the capacitance measured results from oxidation/reduction of the oxide on the electrode.

CONCLUSIONS

In studying the oxygen evolution reaction on cobalt or cobalt-containing oxides many authors did not make a distinction between the behaviour at low and high overpotentials. Our results, however, clearly make such a distinction necessary. Also in some studies the reaction order was measured at low hydroxyl activities (below 1 *M* KOH) but the results were applied to the reaction in 6 *M* KOH. In our investigation of the oxygen evolution on cobalt electrodes we have shown that in the reaction order studies the influence of the water activity may not be neglected. If it is taken into account, a useful extra criterion is obtained to test possible reaction mechanisms. From our measurements we conclude that the following mechanism

holds for the OER on cobalt in the low overpotential region:

$$CoO + OH^- \leftrightarrows CoOOH + e^- \quad \text{(IV.1)}$$

$$CoOOH + OH^- \leftrightarrows CoO_2^- + H_2O \quad \text{(IV.2)}$$

$$CoO_2^- \leftrightarrows CoO_2 + e^- \quad \text{(IV.3)}$$

$$CoO_2 \leftrightarrows CoO + O_{ad} \quad \text{(IV.4)}$$

$$2\ O_{ad} \rightarrow O_2 \quad \text{(IV.5)}$$

This mechanism would explain the experimental results found in our study for low overpotentials when the third step is taken as the rds while steps (IV.1) and (IV.2) are at quasi-equilibrium (with low "coverages") and steps (IV.4) and (IV.5) are fast. At high overpotentials the reaction becomes more difficult to elucidate. For this potential region, the results from anodic polarization and the impedance results are contradictory; from the capacitance data it may be concluded that in the potential range where the Tafel slope changes, an oxidation of the surface oxides take place.

REFERENCES

1 G. Grube and O. Feucht, Z. Elektrochem., 28 (1922) 568.
2 A.G.C. Kobussen and C.M.A.M. Mesters, J. Electroanal. Chem., 115 (1980) 131.
3 S.M. Jasem and A.C.C. Tseung, J. Electrochem. Soc., 126 (1979) 1353.
4 C. Iwakura, A. Honji and H. Tamura, Electrochim. Acta, 26 (1981) 1319.
5 A.N. Krasil'shchikov, Zh. Fiz. Khim., 37 (1963) 531.
6 F.R. van Buren, G.H.J. Broers and T.G.M. van der Belt, Ber. Bunsenges. Phys. Chem. 83 (1979) 82.
7 M. Moors and G. Demedts, J. Phys. E, 9 (1976) 1087.
8 A.G.C. Kobussen, J. Electroanal. Chem., 126 (1981) 199.
9 C. Akerlof and P. Bender, J. Am. Chem. Soc., 70 (1948) 2366.
10 L.d. Burke, M.E. Lyons and O.J. Murphy, J. Electroanal. Chem., 132 (1982) 247.
11 H. Gomez Meier, J.R. Vilche and A.J. Arvia, J. Electroanal. Chem., 138 (1982) 367.
12 G. Bronoel and J. Reby, Electrochim. Acta, 25 (1980) 973.
13 P. Rasiyah and A.C.C. Tseung, J. Electrochem. Soc., 129 (1982) 1724.
14 P. Rasiyah and A.C.C. Tseung, J. Electrochem. Soc., 130 (1983) 365.
15 G.W. Simmons, E. Kellerman and H. Leidheiser, Jr., J. Electrochem. Soc., 123 (1976) 1276.
16 B.D. Cahan and T.C. Chen, J. Electrochem. Soc., 129 (1982) 700.
17 C.T. Chen and B.D. Cahan, J. Electrochem. Soc., 129 (1982) 17.
18 B.D. Cahan and C.T. Chen, J. Electrochem. Soc., 129 (1982) 474.
19 B.D. Cahan and C.T. Chen, J. Electrochem. Soc., 129 (1982) 921.
20 C. Delmas, C. Fouassier and P. Hagenmuller, J. Solid State Chem., 13 (1975) 165.
21 A.G.C. Kobussen and G.H.J. Broers, J. Electroanal. Chem., 126 (1981) 221.
22 A.G.C. Kobussen, H. Willems and G.H.J. Broers, J. Electroanal. Chem., 142 (1982) 67.